

An automatic processing framework for hyperspectral histologic images and benchmark dataset

Ling Ma ^{a,b}, Amie Ha ^{a,b}, Ifrah Zainab ^{a,b}, Armand Rathgeb ^{a,b}, Hasan Mubarak ^{a,b}, Baowei Fei ^{a,b,c*}

^a Center for Imaging and Surgical Innovation, University of Texas at Dallas, Richardson, TX

^b Department of Bioengineering, University of Texas at Dallas, Richardson, TX

^c Department of Radiology, University of Texas Southwestern Medical Center, Dallas, TX

*Corresponding author: bfei@utdallas.edu, Website: <https://fei-lab.org>

ABSTRACT

Hyperspectral imaging (HSI) is an emerging imaging modality for histopathological applications. However, annotations on RGB histological images are usually used as the reference standard. To use and validate hyperspectral data, it is critical to correlate each hyperspectral image with the corresponding region in a whole-slide image and retrieve accurate tissue label. In this work, we developed a fully automated processing pipeline for hyperspectral histological images. Given a high-resolution digitized whole-slide histological image, the annotation, and a hyperspectral image tile of any region in the slide, the proposed method can locate the HSI tile region in the whole-slide image, crop the RGB image tile and tissue label, and align the RGB tile and tissue label to the HSI tile. With our proposed processing pipeline, we collected and formed a dataset with over 350 whole-slide hyperspectral histological images of human head and neck cancers. The proposed processing pipeline can serve as a general tool for fast and automated hyperspectral histological images, thus facilitating the adaptation of hyperspectral imaging in digital pathology to assist automatic histology diagnosis.

Keywords: Hyperspectral imaging, microscope, preprocessing framework, template matching, pathology, histology

1. INTRODUCTION

Hyperspectral imaging (HSI) is a non-contact and label-free imaging modality that has been emerging in medical applications ¹⁻⁴. The three-dimensional (3D) data cube acquired with HSI contains both the spatial and spectral information of the object, which provide more features to help improve the diagnosis or surgical outcome. Previous works have investigated HSI with microscopy for cancer detection ⁵⁻⁸. However, most existing hyperspectral histology studies were carried out using relatively small datasets, which hinder comprehensive evaluation of the potential of HSI and advanced machine learning algorithms. A few recent studies employed HSI with whole-slide imaging (WSI) ⁹⁻¹², which further proved the potential of HSI in histology. Nevertheless, there is limited access to a large benchmark dataset in the field of hyperspectral histology imaging.

Meanwhile, conventional RGB histological images are widely used for diagnosis, which are what pathologists are trained on. Pathological reference standards are usually provided by pathologists outlining the disease region on digitized histological images. Retrieving the correct ground truth from annotations on the whole-slide RGB images for each hyperspectral image is critical to evaluate the performance of classification and segmentation methods with HSI data. In addition, our previous work ¹² showed that acquiring low-resolution hyperspectral images and fusing with high-resolution RGB to reconstruct high-resolution HSI has several advantages, such as faster image acquisition, less burden of data storage, and good image quality. Therefore, combining digitized RGB histological images with HSI represents a new research direction in this area.

Therefore, we aim to fulfill a high-speed and high-quality hyperspectral whole-slide histology imaging workflow, which would allow the standardized acquisition and versatile utilization of a hyperspectral histologic imaging, as shown in Figure 1. The approaches for automated hyperspectral image acquisition and super-resolution reconstruction have been developed in our previous work ¹². In this study, we improved our automated hyperspectral microscopic imaging system and proposed a preprocessing framework, which could automatically locate and crop the corresponding region of the

hyperspectral image from the RGB WSI, as well as retrieve pixel-level reference standard from pathologist's annotation. The cropped RGB tiles can be registered to the corresponding hyperspectral images for super-resolution reconstruction, while the retrieved pixel-level reference standard can facilitate the evaluation of HSI classification and segmentation. The framework serves as a general tool to assist the use of hyperspectral data. Based on this proposed processing pipeline and our developed automated hyperspectral microscope system, we scanned over 350 whole slides with standardized acquisition parameters and established a dataset of hyperspectral WSIs of human head and neck cancers.

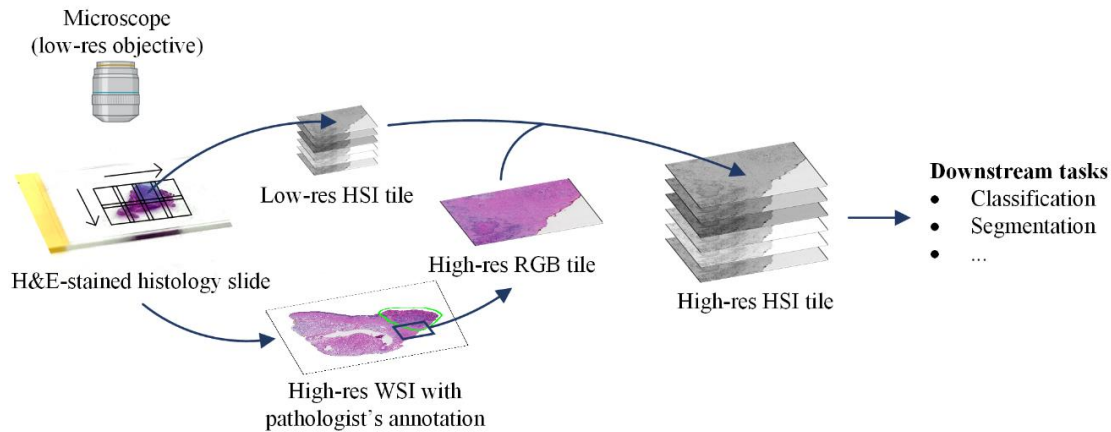


Figure 1. Proposed workflow of high-speed hyperspectral histology imaging.

2. METHODS

2.1 Automated hyperspectral whole-slide imaging system

In our previous work¹², an automated hyperspectral whole-slide imaging system based on an upright brightfield microscope was implemented, which synchronizes the motorized stage and hyperspectral camera for whole-slide scanning and automatically focus based on an additional RGB camera. In this work, we refined the system and developed an automated hyperspectral whole-slide imaging microscope that includes a customized snapscan hyperspectral camera and a fully motorized inverted microscope. Only one hyperspectral camera was mounted on the side video port of the microscope, adding minimum complexity to the entire setup. Software has been developed to implement autofocus based on the hyperspectral camera itself as well as to control the microscope and camera for automated whole-slide scanning. In order to reduce the slide scanning time and the data storage space on hard drives, we acquired low-resolution hyperspectral images with our lowest power objective lens available, *i.e.*, 4 \times , with a 0.5 \times C-mount video adapter for the camera. Since the hyperspectral camera has a larger sensor size that is almost double the normal RGB camera sensor, our low-resolution hyperspectral images had an optical resolution that is close to RGB histological images acquired with a 4 \times objective. Furthermore, we used the integrated 100-Watt halogen light source for a bright and relatively uniform illumination.

2.2 Standardized data acquisition

The hyperspectral images had an image resolution of 1000 pixels \times 1000 pixels with a field of view (FOV) of approximately 2740 μm \times 2740 μm . Each image contained 87 bands in the wavelength range of 470-720 nm. The step size of whole-slide scanning was set to 2500 μm , with which the adjacent hyperspectral images would have just sufficient overlap for whole-slide reconstruction. Our developed microscopic system has an auto-focus feature, which scans along the z axis and finds the best focus within a second. The illumination was set to half of the maximum intensity of the halogen light source, and the hyperspectral camera integration time was 0.1 ms. We acquired one white reference image for each whole slide, and all hyperspectral image tiles from the same slide were calibrated using one white reference. Furthermore, ambient light was turned off while imaging. With all the acquisition parameters being identical, *i.e.*, illumination, integration time, objective magnification, video adapter magnification, and scanning step size, we aimed to collect a standardized dataset with good data generalization.

The RGB digitized histological images used in this work were acquired from our previous work with a whole-slide scanner at 40× objective magnification¹³. They were originally saved as NDPI files, but for each scanned whole slide we exported a TIFF file, which maintained the original image resolution and the best possible image quality.

2.3 Automatic preprocessing pipeline

In this study, we developed an automatic pipeline for the processing of large volume of hyperspectral data obtained from automated hyperspectral whole-slide scanning, in order to generate standardized benchmark hyperspectral histology dataset. For each scanned whole histologic slide, we obtain many hyperspectral image tiles (varying from 6 to 72, average 18), each of which is a 1000 pixel × 1000 pixel hypercube taken at one location. We also export a full-resolution RGB image from the digitized histological image. In addition, a screenshot of the whole slide with pathologist’s annotation is saved, which would be converted to a pixel-level tissue label mask and registered to the high-resolution RGB histology whole-slide image. All hyperspectral tiles from the same whole slide are calibrated using one white reference image. Then, all tiles go through a quality check to get rid of the ones without sufficient tissue or out of focus. For each of the good tiles, the pipeline would automatically find the corresponding region in the RGB whole-slide image using template matching. Then, a tile of a slightly larger region is cropped from the whole-slide RGB as well as the registered tissue label mask, respectively. Finally, we register the cropped RGB and the mask tiles to the HSI tile but maintain the high-resolution. Eventually, each HSI tile would have a corresponding high-resolution RGB tile and a pixel-level tissue label mask tile. The RGB tiles can be used for either visualization or super-resolution reconstruction, while the labels can be used to train classification or segmentation networks using the hyperspectral data. The processing pipeline is illustrated in Figure 2, and the details are described below.

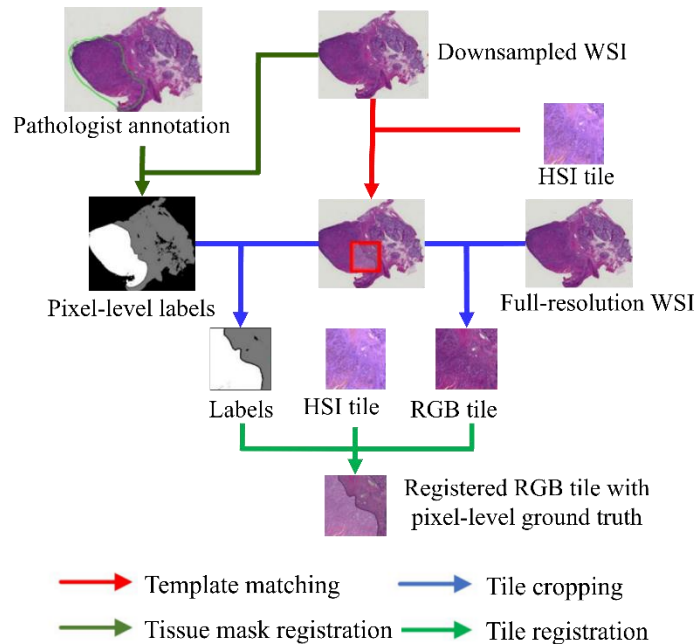


Figure 2. Standardized acquisition and preprocessing framework of hyperspectral histological images.

2.3.1 Hyperspectral image tile quality check

During the whole-slide scanning, the camera scans a defined rectangular region on the slide. Due to the irregular shape of the tissue samples, there are usually plenty of blank image tiles. Keeping these tiles would take up lots of unnecessary space on hard drives. In addition, when there is very little tissue in a tile, our auto-focus algorithm might not work perfectly, resulting in a blurry image. Therefore, it is necessary to run a quality check of all HSI tiles and get rid of the blank or out-of-focus ones before forming the benchmark dataset.

The H&E-stained tissue has very strong absorption in the 525-540 nm wavelength range, leading to a high contrast between tissue and background in the 21st to the 25th bands. By applying a hard threshold to the average of 21st to 25th bands, the tissue can be easily segmented, as shown in Figure 3 (a-c). Then, we calculated the area of the segmented tissue in the tile. If the area was smaller than 60×60 pixels, the tile would be regarded as blank and discarded. If the tile had sufficient tissue, a bounding box is generated to extract the tissue region, and a Brenner score¹⁰ of the region is calculated to evaluate the focus. If the Brenner score is lower than 75, the tile will be regarded as out-of-focus and be rescanned. Some examples of the tiles that have been removed from the dataset are shown in Figure 3 (d-f).

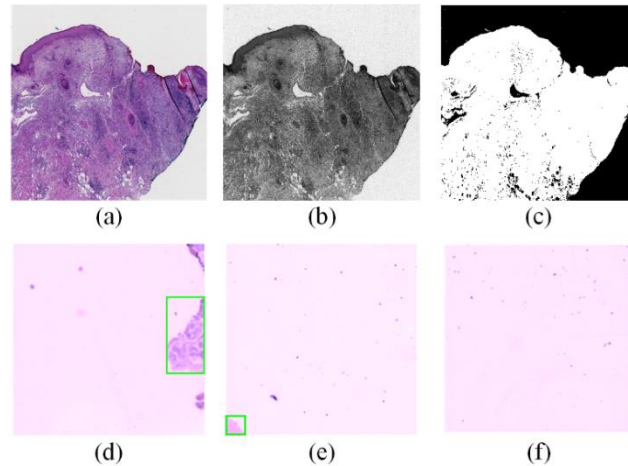


Figure 3. Hyperspectral tile quality check. (a) RGB histologic image of a tile with sufficient tissue. (b) Average of the 21st to 25th bands in the HSI tile, which gives good contrast between tissue and background for segmentation. (c) Tissue segmentation mask using the averaged bands. (d) An HSI tile with the unfocused region outlined by a green box, which required rescanning. (e) An HSI tile with insufficient and unfocused tissue, thus being removed from the dataset. (f) An HSI tile with no tissue but only scatters of staining, thus being removed from the dataset.

2.3.2 Annotation and tissue mask

In order to retrieve the accurate labels for tissues, we first convert the pathologist’s annotation to a tissue mask and register it to the whole-slide histological image. A threshold was set to the red, green, and blue bands of the annotation image to segment the tissue. Meanwhile, another threshold was applied to extract the annotation. Then, two masks were merged together using bitwise AND operation, in order to generate a tissue mask, where white (grayscale intensity 1) indicates cancerous tissue, gray (grayscale intensity 0.5) means normal tissue, and black (grayscale intensity 0) means no tissue. Because the screenshot of annotation had a different (and much lower) image resolution than the full-resolution whole-slide image, the generated tissue mask cannot be directly applied. Thus, we register the annotation image to the full-resolution WSI and apply the registration matrix to the merged mask, which yields a pixel-level whole-slide tissue label image. The process is illustrated by the dark green lines in Figure 2 and the detailed flow is shown in Figure 4.

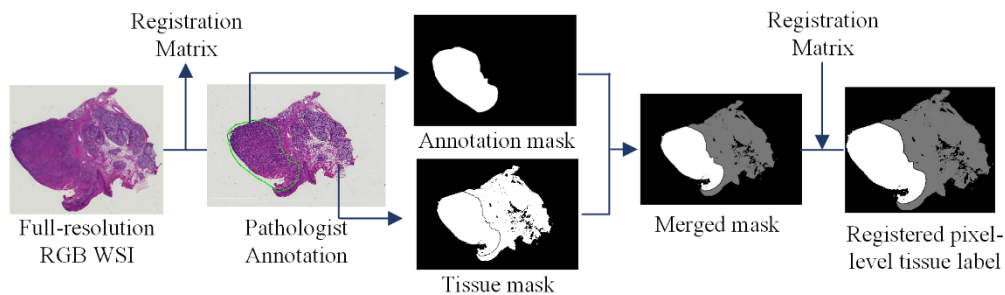


Figure 4. Extract pathological ground truth and generate pixel-level whole-slide tissue labels.

2.3.3 Template matching

The most important job of our proposed processing pipeline is to automatically locate the region of HSI tile in the whole-slide image. As pathologists give ground truth annotation on RGB histological images, it is necessary to accurately locate the HSI tile for the correct labels, especially when the tissue is at the tumor-normal margin. When dealing with a large number of hyperspectral tiles, or in the circumstance where a random region of interest was imaged, an automatic tool to locate the HSI tile would be very helpful.

In this work, we used template matching from the OpenCV package to locate each HSI tile. For faster calculation, we first downsampled the full-resolution whole-slide image 10 times to a low-resolution WSI, which is equivalent to 4× objective magnification. Then, both the downsampled WSI and the HSI tile were converted to grayscale, and the HSI tile was used as the “template”. Various template matching methods including 'TM_CCOEFF', 'TM_CCOEFF_NORMED', 'TM_CCORR', 'TM_CCORR_NORMED', 'TM_SQDIFF', and 'TM_SQDIFF_NORMED' were tested, and the 'TM_CCOEFF_NORMED' method gave the best matching results. In addition, considering the slightly different optical resolution of the downsampled WSI and the HSI tiles, we resized the HSI tiles by different factors, such as 1.1 to 1.2 with 0.01 increment, and used each resized tile as a template. Moreover, to increase the template matching performance for tiles near the edge of the slide, we expanded the WSI by padding 1000 pixels on four edges of the image. Eventually, the one that resulted in the highest template matching score would be used, and the bounding box of the region would be generated, as shown by the red route in Figure 2. If the template matching score was lower than a certain threshold, it would be determined that no matching was achieved. For this type of rare cases, we would revisit the tiles and see if it was caused by compromised focus or other possible image artifacts.

2.3.4 Automatic cropping and registration

Once the corresponding region of HSI tile is located from the RGB whole-slide image, a slightly larger RGB tile as well as a tissue mask tile would be cropped. Then, the high-resolution RGB tile was registered to the HSI tile using affine registration with the Oriented FAST and Rotated BRIEF (ORB) feature detector from the OpenCV package. Note that the HSI tiles were 1000×1000 pixels acquired at 4× objective magnification, while the full-resolution RGB histological image was acquired at 40× objective magnification. Thus, the RGB tile was first downsampled 10 times to match the resolution of the HSI tile. Once the registration matrix was obtained, we could apply a scaling factor to the matrix and generate a RGB tile of any resolution while keeping the RGB and HSI tiles aligned. Meanwhile, by applying the same matrix to the tissue mask tile, we could obtain pixel-level labels of the HSI and RGB tiles. The labels can be used to train a classification or segmentation network using the HSI data. The automatic cropping and registration are shown by the blue and light green routes in Figure 2.

3. RESULTS

With the standardized data acquisition and automated processing pipeline, we have collected hyperspectral data of 198 whole slides from 70 squamous cell carcinoma (SCC) patients and 178 whole slides from 70 thyroid cancer patients. Our pipeline was run in a single thread on an AMD EPYC 7002 series processor.

Table 1. Benchmark dataset of whole-slide hyperspectral histologic images of human head and neck cancers

	SCC	Thyroid
Total No. of slides	198	178
Total No. of patients	70	70
Average No. of tiles	15 ± 7.7	22 ± 12.8
Average scanning time (min)	17.2 ± 9.6	23.6 ± 13.6
Average scanning area (mm ²)	53.8 ± 38.5	89.2 ± 64.7

The template matching and automatic registration performance of our processing pipeline is shown in Figure 5 for an SCC tumor-normal margin slide and Figure 6 for a thyroid tumor-normal slide, respectively. It can be seen that the tissue label mask perfectly segmented the tissue while separating the tumor, normal tissue, and background. For the HSI tiles in Figure 5(c) and Figure 6(c), our method located the corresponding regions in the whole-slide images, cropped the RGB tiles and tissue label masks, and aligned them with the HSI tiles. Note that the HSI tiles were acquired with 4× objective magnification while the RGB images were scanned with 40× objective. Since the HSI tiles had an image resolution of 1000×1000 pixels, we obtained RGB tiles and tissue label masks of 10,000 × 10,000 pixels resolution, in order to keep the most detailed spatial information. Nevertheless, they can be downsampled to any magnification for different applications. Most importantly, the pixel-level tissue label mask can facilitate the use of large amount of hyperspectral data, such as training neural networks for classification or segmentation.

In order to further validate the effectiveness of our entire workflow, we reconstructed high-resolution hyperspectral patches using the automatically registered low-resolution HSI tile and high-resolution RGB tile, as shown in Figure 7. Even though the original HSI tile was acquired at a very low resolution (4× objective magnification) with barely any pathological features, our reconstructed high-resolution hyperspectral image shows the same level of morphological details as the digitized RGB images in addition to its intrinsic rich spectral features. For a more straightforward comparison, we scanned a few whole slides using a 10× objective lens and a 40× objective lens as well. For the whole slide that was scanned with both 4× and 10× objective lens, using 4× resulted in a total number of 14 HSI tiles (after removing no-tissue tiles) that took 979 Mb storage space when saved in unsigned int8 format, while using 10× resulted in a total number of 62 HSI tiles that took 4.99 Gb with the same format. For the slide that was scanned using 4× and 40× objective lenses, scanning a 15 mm × 12.5 mm region using 4× lens resulted in 31 HSI tiles (2.18 Gb), while scanning only 1.75 mm × 1.5 mm region using the 40× lens could already yield 69 tiles (5.35 Gb). Overall, it is more cost effective to use our proposed workflow for the acquisition of a large benchmark hyperspectral histology dataset.

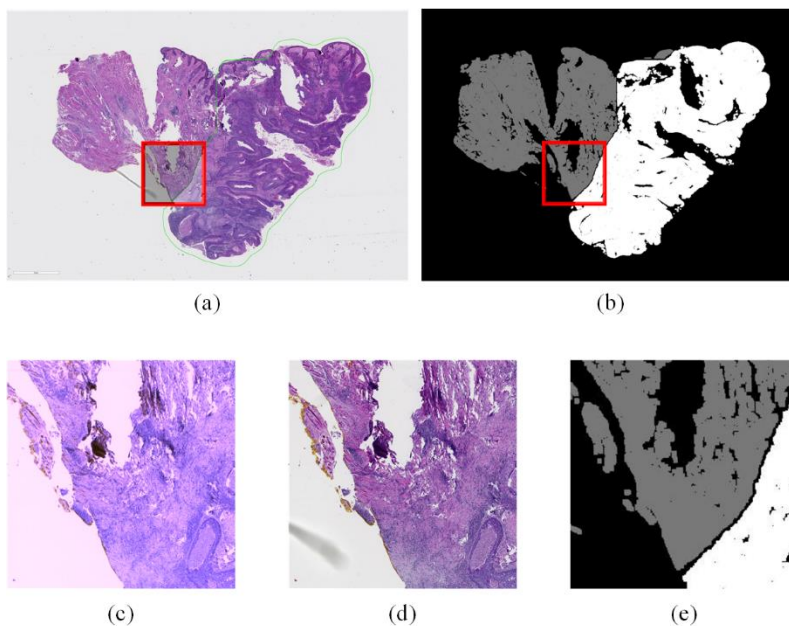


Figure 5. Automatic cropping and ground truth retrieval of an HSI tile of SCC slide. (a) Digitized WSI with pathologist’s annotation of an SCC cancer margin tissue. (b) Pixel-level tissue label mask, where white means cancerous tissue, gray means normal tissue, and black means blank slide with no tissue. (c) A hyperspectral tile of the cancer-normal margin region, as marked by the red box in (a) and (b). The image tile has a resolution of 1000×1000 pixels. (d) Automatically cropped and registered high-resolution RGB tile with an image resolution of 10,000×10,000 pixels. (e) Automatically cropped and registered pixel-level label mask with an image resolution of 10,000×10,000 pixels.

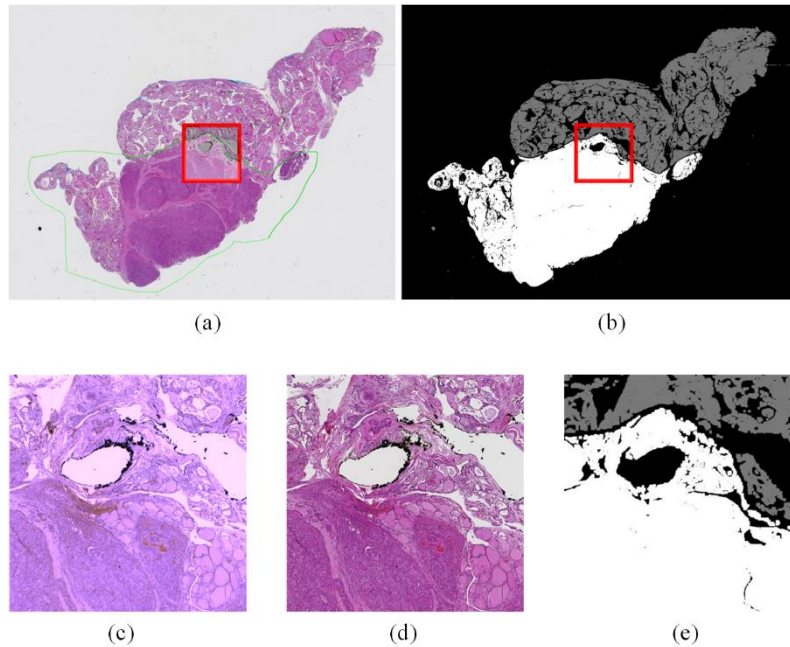


Figure 6. Automatic cropping and ground truth retrieval of an HSI tile of thyroid slide. (a) Digitized WSI with pathologist's annotation of a thyroid cancer margin tissue. (b) Pixel-level tissue label mask, where white means cancerous tissue, gray means normal tissue, and black means blank slide with no tissue. (c) A hyperspectral tile of the cancer-normal margin region, as marked by the red box in (a) and (b). The tile has an image resolution of 1000×1000 pixels. (d) Automatically cropped and registered high-resolution RGB tile with an image resolution of $10,000 \times 10,000$ pixels. (e) Automatically cropped and registered pixel-level label mask with an image resolution of $10,000 \times 10,000$ pixels.

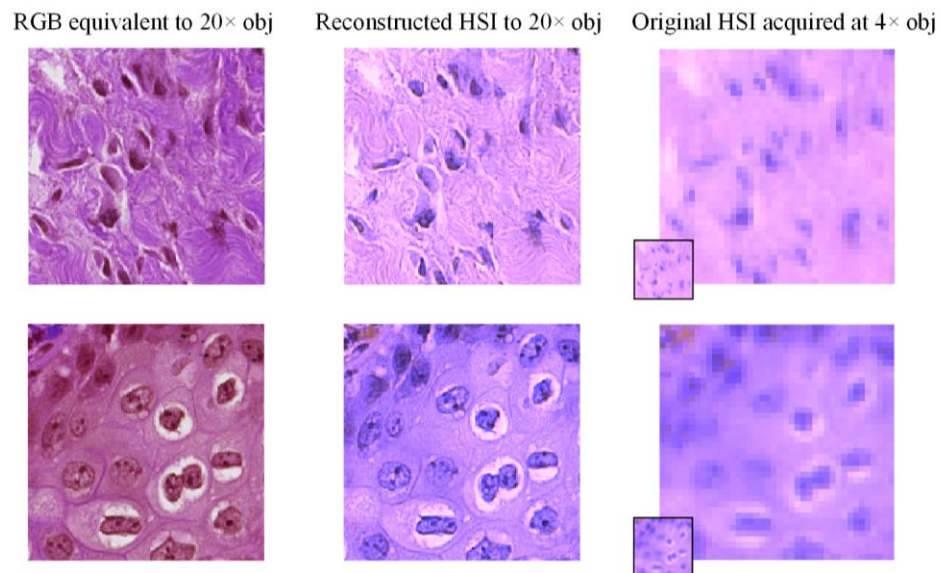


Figure 7. Super-resolution reconstruction of hyperspectral image patches from the original resolution of $4 \times$ objective magnification to a higher resolution equivalent to $20 \times$ objective magnification. For the original HSI patches, the small patches at bottom left are original image size, with zoomed-in ones showing the lack of spatial information. Top row: an HSI patch from a normal slide. Bottom row: an HSI patch from a tumor slide.

4. DISCUSSION & CONCLUSION

In this study, we proposed to seamlessly integrate hyperspectral imaging into histopathological workflow and created benchmark hyperspectral dataset by implementing hyperspectral whole-slide histology imaging. We developed an automated whole-slide hyperspectral microscope system as well as a fully automatic pipeline to process large volumes of microscopic hyperspectral images, which is capable of aligning each hyperspectral image tile to the corresponding region in the whole-slide RGB histological image and retrieving its pixel-level reference standard from the pathologist's annotation. Based on this framework, we employed standardized acquisition parameters and obtained a comprehensive benchmark dataset of whole-slide hyperspectral histological images of human head and neck cancers. Combined with our hyperspectral super-resolution reconstruction method, we obtained high-quality hyperspectral histological images of various magnifications for different purposes.

In the future, we will expand this processing pipeline to more imaging modalities, such as polarized hyperspectral imaging and fluorescence hyperspectral imaging, as they are often used to scan a small region of the slide, thus in better need of automatic retrieval of the ground truth from whole-slide annotations. Overall, our image acquisition and processing pipeline would significantly boost the acquisition speed and data generalization of hyperspectral histological images, thus promoting the adaptation of HSI in histological imaging.

ACKNOWLEDGMENTS

Research reported in this publication was supported in part by the National Cancer Institute of the National Institutes of Health under Award Number R01CA288379 and R01CA204254 and by the Cancer Prevention and Research Institute of Texas (CPRIT) under Award Number RP240289 and RP240542. The content is solely the responsibility of the authors and does not necessarily represent the official views of the National Institutes of Health.

DISCLOSURES

The authors have no relevant financial interests in this article and no potential conflicts of interest to disclose.

REFERENCES

- [1] Lu, G., and Fei, B., "Medical hyperspectral imaging: a review," *Journal of biomedical optics*, 19(1), 010901 (2014).
- [2] Ortega, S., Halicek, M., Fabelo, H., Callico, G. M., and Fei, B., "Hyperspectral and multispectral imaging in digital and computational pathology: a systematic review," *Biomedical Optics Express*, 11(6), 3195-3233 (2020).
- [3] Halicek, M., Fabelo, H., Ortega, S., Callico, G. M., and Fei, B., "In-vivo and ex-vivo tissue analysis through hyperspectral imaging techniques: revealing the invisible features of cancer," *Cancers*, 11(6), 756 (2019).
- [4] Tran, M. H., and Fei, B., "Compact and ultracompact spectral imagers: technology and applications in biomedical imaging," *Journal of Biomedical Optics*, 28(4), 040901 (2023).
- [5] Ma, L., Little, J., Chen, A., Myers, L., Sumer, B., and Fei, B., "Automatic detection of head and neck squamous cell carcinoma on histologic slides using hyperspectral microscopic imaging," *Journal of Biomedical Optics*, 27(4), 046501 (2022).
- [6] Du, J., Tao, C., Xue, S., and Zhang, Z., "Joint Diagnostic Method of Tumor Tissue Based on Hyperspectral Spectral-Spatial Transfer Features," *Diagnostics (Basel)*, 13(12), (2023).
- [7] Cinar, U., Cetin Atalay, R., and Cetin, Y. Y., "Human Hepatocellular Carcinoma Classification from H&E Stained Histopathology Images with 3D Convolutional Neural Networks and Focal Loss Function," *J Imaging*, 9(2), (2023).
- [8] Maktabi, M., Wichmann, Y., Köhler, H., Ahle, H., Lorenz, D., Bange, M., Braun, S., Gockel, I., Chalopin, C., and Thieme, R., "Tumor cell identification and classification in esophageal adenocarcinoma specimens by hyperspectral imaging," *Scientific Reports*, 12(1), 1-14 (2022).

- [9] Tran, M. H., Gomez, O., and Fei, B., "A video transformer network for thyroid cancer detection on hyperspectral histologic images." Proc. SPIE 12471, Medical Imaging 2023: Digital and Computational Pathology, 1247107 (2023).
- [10] Tran, M. H., Gomez, O., and Fei, B., "An automatic whole-slide hyperspectral imaging microscope," Proc. SPIE 12391, Label-free Biomedical Imaging and Sensing (LBIS) 2023, 1239106, (2023).
- [11] Tran, M. H., Ma, L., Litter, J. V., Chen, A. Y., and Fei, B., "Thyroid Carcinoma Detection on Whole Histologic Slides Using Hyperspectral Imaging and Deep Learning," Proc SPIE Int Soc Opt Eng, 12039, (2022).
- [12] Ma, L., Rathgeb, A., Mubarak, H., Tran, M., and Fei, B., "Unsupervised super-resolution reconstruction of hyperspectral histology images for whole-slide imaging," Journal of Biomedical Optics, 27(5), 056502 (2022).
- [13] Halicek, M., Shahedi, M., Little, J. V., Chen, A. Y., Myers, L. L., Sumer, B. D., and Fei, B., "Head and Neck Cancer Detection in Digitized Whole-Slide Histology Using Convolutional Neural Networks," Scientific Reports, 9(1), 14043 (2019).